miR-182 targeting reprograms tumor-associated macrophages and limits breast cancer progression

Chengxin Ma[a], Dasa He[a], Pu Tian[a], Yuan Wang[a], Yunfei He[a], Qiuyao Wu[a], Zhenchang Jia[a], Xue Zhang[a], Peiyuan Zhang[a] (ORCID), Hao Ying[a], Zi-Bing Jin[b] (ORCID), and Guohong Hu[a,1]

[a]Shanghai Institute of Nutrition and Health, University of Chinese Academy of Sciences, Chinese Academy of Sciences, Shanghai 200031, China; and [b]Beijing Institute of Ophthalmology, Beijing Tongren Hospital, Capital Medical University, Beijing Key Lab of Ophthalmology and Visual Sciences, Beijing 100005, China

The protumor roles of alternatively activated (M2) tumor-associated macrophages (TAMs) have been well established, and macrophage reprogramming is an important therapeutic goal. However, the mechanisms of TAM polarization remain incompletely understood, and effective strategies for macrophage targeting are lacking. Here, we show that miR-182 in macrophages mediates tumor-induced M2 polarization and can be targeted for therapeutic macrophage reprogramming. Constitutive miR-182 knockout in host mice and conditional knockout in macrophages impair M2-like TAMs and breast tumor development. Targeted depletion of macrophages in mice blocks the effect of miR-182 deficiency in tumor progression while reconstitution of miR-182-expressing macrophages promotes tumor growth. Mechanistically, cancer cells induce miR-182 expression in macrophages by TGFβ signaling, and miR-182 directly suppresses *TLR4*, leading to NFκb inactivation and M2 polarization of TAMs. Importantly, therapeutic delivery of antagomiR-182 with cationized mannan-modified extracellular vesicles effectively targets macrophages, leading to miR-182 inhibition, macrophage reprogramming, and tumor suppression in multiple breast cancer models of mice. Overall, our findings reveal a crucial TGFβ/miR-182/TLR4 axis for TAM polarization and provide rationale for RNA-based therapeutics of TAM targeting in cancer.

miR-182 | tumor-associated macrophage | breast cancer | RNAi therapeutics | extracellular vesicle

It is well known that the nonmalignant stromal components in tumors play pivotal roles in tumor progression and therapeutic responses (1, 2). Macrophages are a major component of tumor microenvironment and display considerable phenotypic plasticity in their effects toward tumor progression (3–5). Classically activated (M1) macrophages often exert direct tumor cytotoxic effects or induce antitumor immune responses by helping present tumor-related antigens (6, 7). In contrast, tumoral cues can polarize macrophages toward alternative activation with immunosuppressive M2 properties (6–8). Numerous studies have firmly established the protumor effects of M2-like tumor-associated macrophages (TAMs) and the association of TAMs with poor prognosis of human cancer (9–11). However, how tumors induce the coordinated molecular and phenotypic changes in TAMs for M2 polarization remains incompletely understood, impeding the designing of TAM-targeting strategies for cancer intervention. In addition, drug delivery also represents a hurdle for therapeutic macrophage reprogramming.

Noncoding RNAs, including microRNAs, have been shown to play vital roles in various pathological processes of cancer (12). The microRNA miR-182 has been implicated in various developmental processes and disease conditions (13–15). Particularly, it receives extensive attention in cancer studies. Prevalent chromosomal amplification of miR-182 locus and up-regulation of its expression in tumors have been observed in numerous cancer types including breast cancer, gastric cancer, lung adenocarcinoma,

colorectal adenocarcinoma, ovarian carcinoma, and melanoma (16–21). miR-182 expression is also linked to higher risk of metastasis and shorter survival of patients (20, 22–24). Functional studies showed that miR-182 expression in cancer cells plays vital roles in various aspects of cancer malignancy, including tumor proliferation (25–29), migration (30, 31), invasion (16, 32, 33), epithelial-mesenchymal transition (34–36), metastasis (21, 37, 38), stemness (30, 39, 40), and therapy resistance (41, 42). A number of target genes, including FOXO1/3 (18, 21, 43–45), *CYLD* (46), *CADM1* (47), *BRCA1* (27, 48), *MTSS1* (34), *PDK4* (49), and *SMAD7* (35), were reported to be suppressed by miR-182 in cancer cells. Our previous work also proved that tumoral miR-182 regulates lipogenesis in lung adenocarcinoma and promotes metastasis of breast cancer (34, 35, 49). Although miR-182 was established as an important regulator of cancer cell malignancy, previous studies were limited, with analyses of miR-182 in cultured cancer cells and transplanted tumors. Thus, the consequences of miR-182 regulation in physiologically relevant tumor models, such as genetically modified mice, have not been shown. More importantly, whether miR-182 also plays a role in tumor microenvironmental cell components is unknown.

In this study, we show that miR-182 expression in macrophages can be induced by breast cancer cells and regulates

Significance

Breast cancer is a major threat of women's health worldwide. Nontumor cell components play crucial roles in cancer. Macrophages, the cells of the innate immune system that normally exert antitumor activities, can be educated by tumors to an alternatively activated phenotype that is known to promote tumor progression. Understanding the mechanism of macrophage education by tumor cells will help the design of new therapeutic approaches. We find that breast tumor cells induce the expression of a microRNA, miR-182, in macrophages, and miR-182 promotes macrophage alternative activation to drive tumor development. Importantly, using cationized mannan-modified extracellular vesicles to load miR-182 inhibitors and deliver the inhibitors specifically into macrophages can effectively inhibit alternative activation of macrophages and suppress breast tumor development.

TAM polarization in various tumor models of mice. In addition, miR-182 inhibition with TAM-targeting exosomes demonstrates promising efficacy for cancer treatment.

Results

miR-182 Deficiency in Mice and Macrophages Impairs M2 Polarization of TAMs and Progression of Breast Cancer. Previous studies established the oncogenic roles of miR-182 in cancer cells. Interestingly, we also observed higher miR-182 expression in M2 macrophages derived from THP1 monocytes as compared to naïve (M0) or M1 macrophages (*SI Appendix*, Fig. S1*A*). Reanalyses of previously published transcriptomic sequencing datasets (51, 52) also demonstrated marked miR-182 up-regulation in human and murine M2 macrophages and TAMs of breast cancer (Fig. 1 *A* and *B*). Further, we analyzed miR-182 expression by fluorescence in situ hybridization (FISH) and TAM infiltration by immunofluorescent (IF) staining in a cohort of human breast tumors. The analysis revealed a significant correlation of miR-182 expression and CD206$^+$ macrophage

enrichment in human tumors (Fig. 1*C*). These data implicated a role of miR-182 in TAMs of breast cancer.

Thus, we used several mouse models to assess the role of miR-182 in macrophages and breast cancer development. First, we utilized a previously reported constitutive miR-182 knockout (KO) mouse model (52). The genetic locus of miR-182 was replaced by the neomycin-encoding sequence (*SI Appendix*, Fig. S1*B*), leading to miR-182 deficiency in various tissues of the mice (*SI Appendix*, Fig. S1*C*). Consistent with the previous study (52), the KO mice were viable and fertile and exhibited no gross phenotypic abnormalities compared to their wild-type littermates. Notably, mammary glands from the wild-type and KO mice showed no obvious differences in numbers of terminal end buds or branches (*SI Appendix*, Fig. S1*D*), indicating that miR-182 is dispensable for normal mammary gland development.

Then, the miR-182-KO and wild-type mice were crossed with the MMTV-PyMT mice, and the macrophages in autochthonous breast tumors were analyzed by flow cytometry (*SI Appendix*, Fig. S1*E*). It was observed that miR-182 deficiency did not affect the total abundance of TAMs in tumor tissues (Fig. 1*D*) but
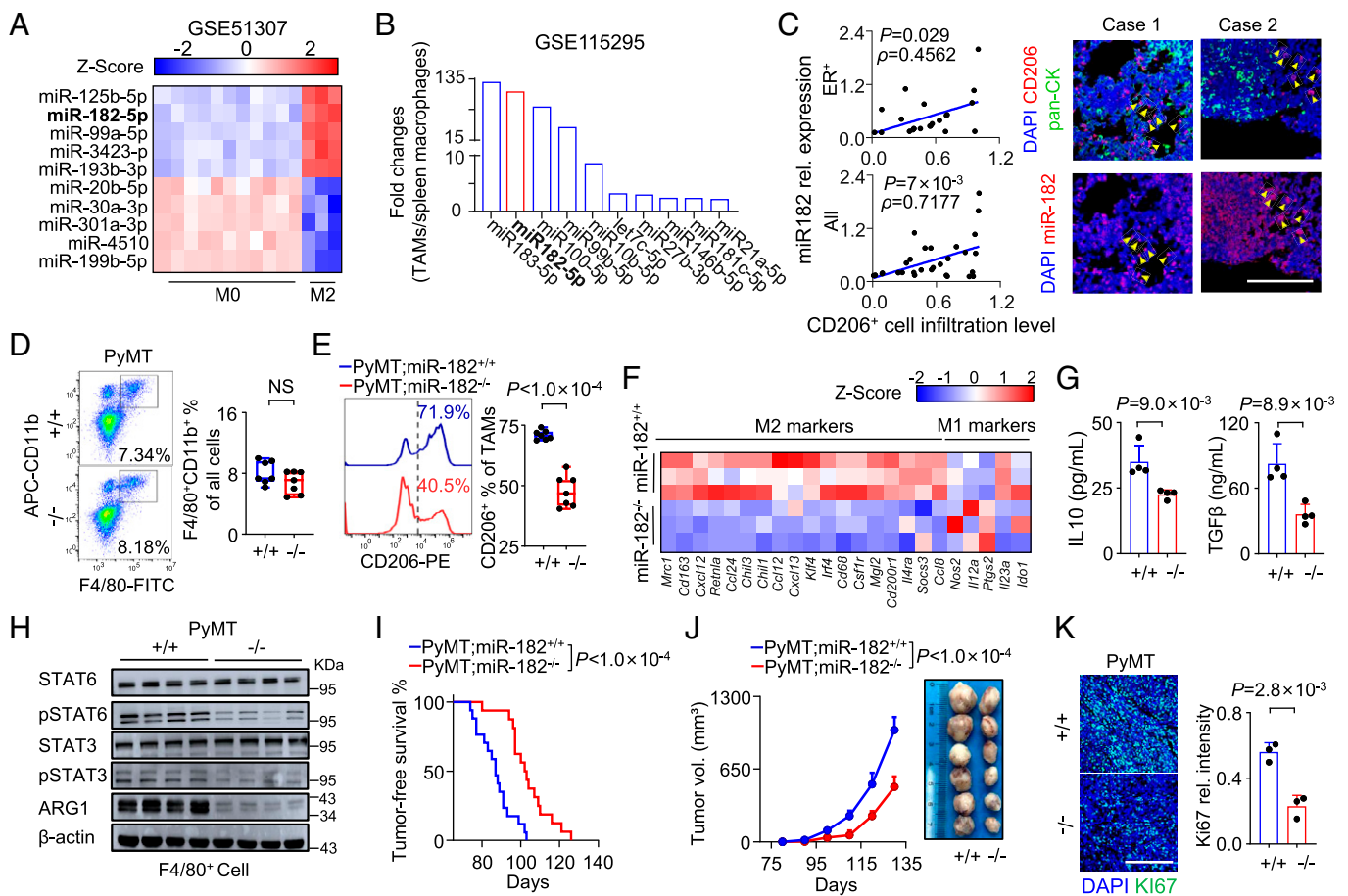

Fig. 1. miR-182 deficiency in mice impairs TAM polarization and breast cancer progression. (*A*) Expression heatmap of the top five up- and down-regulated miRNAs in the human M2 versus M0 macrophages (50) (GSE51307). (*B*) Fold changes of expression of the top 10 up-regulated miRNAs in the TAMs isolated from mouse breast tumors compared with spleen macrophages (51) (GSE115295). (*C*) Correlation of miR-182 expression, detected by FISH, and CD206$^+$ cell infiltration levels, detected by IF staining, in ER$^+$ ($n = 25$ patients) and all ($n = 30$ patients) samples of a human breast cancer cohort. Shown on the right are representative FISH and IF images of two tumors. Arrowheads point to miR-182-expressing CD206$^+$ cells. (*D–K*) Analyses of macrophage polarization and tumor progression in the miR-182-KO (miR-182$^{-/-}$, $^{-/-}$) or wild-type (miR-182$^{+/+}$, $^{+/+}$) mice crossed with MMTV-PyMT mice. Shown are flow cytometric analyses of F4/80$^+$CD11b$^+$ macrophage fraction of all cells in tumors (*D*, $n = 7$ mice each group) and CD206$^+$ fraction in macrophages in tumors (*E*, $n = 7$ mice each group), expression heatmap of M2 and M1-macrophage marker genes of tumors (*F*), ELISA of serological IL-10 and TGFβ levels of the mice (*G*, $n = 4$ mice each group), ARG1 expression and STAT3/6 phosphorylation in F4/80$^+$ cells from the tumors (*H*), animal tumor-free survival rates (*I*, $n = 16$ and 17 mice for KO and wild-type groups), tumor growth (*J*, $n = 16$ and 17 mice for KO and wild-type groups), and Ki67 IF analysis of the tumors (*K*, $n = 5$ tumors each group). *P* values were obtained by Pearson correlation analysis (*C*), two-tailed unpaired *t* test (*D*, *E*, *G*, and *K*), log-rank test (*I*), or two-way ANOVA (*J*). (Scale bar, 50 μm.) Box plots display values of minimum, first quartile, median, third quartile, and maximum (*D* and *E*). Bar graphs show mean + SD (*G* and *K*). Data points show mean + SEM (*J*).

Ma et al.
miR-182 targeting reprograms tumor-associated macrophages and
limits breast cancer progression

caused a significant decrease in the proportion of M2-like CD206^{+} macrophages (Fig. 1E). IF staining also revealed the decrease of CD206^{+} macrophages in the tumors of miR-182-KO mice (*SI Appendix*, Fig. S1F). Consistently, transcriptomic sequencing analysis of the tumor tissues showed that miR-182 deficiency inhibited expression of M2-macrophage marker genes (Fig. 1F). Previously identified gene sets up-regulated in M2 macrophages compared with resting or M1 macrophages (53, 54) were also suppressed in miR-182-KO tumors (*SI Appendix*, Fig. S1G). Furthermore, the concentrations of several anti-inflammatory factors known to be secreted by M2 macrophages, including IL10 and TGFβ but not the M1 cytokine IL12 (55) or GCSF, which can be produced by stromal cells (56), were reduced in the sera of KO mice after tumor appearance (Fig. 1G and *SI Appendix*, Fig. S1H). In addition, when the F4/80[+] macrophages were isolated from the tumors and analyzed, it was found that the M2 markers, including STAT3 and STAT6 phosphorylation, and ARG1 and *Il10* expression were all significantly suppressed in the macrophages of KO tumors (Fig. 1H and *SI Appendix*, Fig. S1I). These data showed that constitutive

miR-182-KO leads to impairment of M2 polarization of macrophages in autochthonous tumors.

Concordant with the well-established protumor roles of M2-like TAMs, deficiency of M2-like TAMs in miR-182-KO mice was accompanied with the suppression of tumor initiation (Fig. 1I), growth (Fig. 1 J and K), and progression (*SI Appendix*, Fig. S1 J and K). Consistent to the role of macrophage miR-182 on tumor progression, we also observed the up-regulation of miR-182 expression in macrophages of lung metastases of MMTV-PyMT (miR-182 wild-type) mice as compared to macrophages in normal lung tissues (*SI Appendix*, Fig. S1L).

To analyze the role of miR-182 in tumor microenvironment rather than in tumor cells, the Py8119 cancer cells, derived from murine PyMT breast tumors, were orthotopically injected into the wild-type and miR-182-KO mice. Again, miR-182-KO in host mice led to reduction of CD206^{+} macrophages but not total macrophages in the transplanted tumors, as shown by flow cytometry (Fig. 2A and *SI Appendix*, Fig. S2A) and IF analyses (Fig. 2B). Serological levels of IL10 and TGFβ, but not IL12
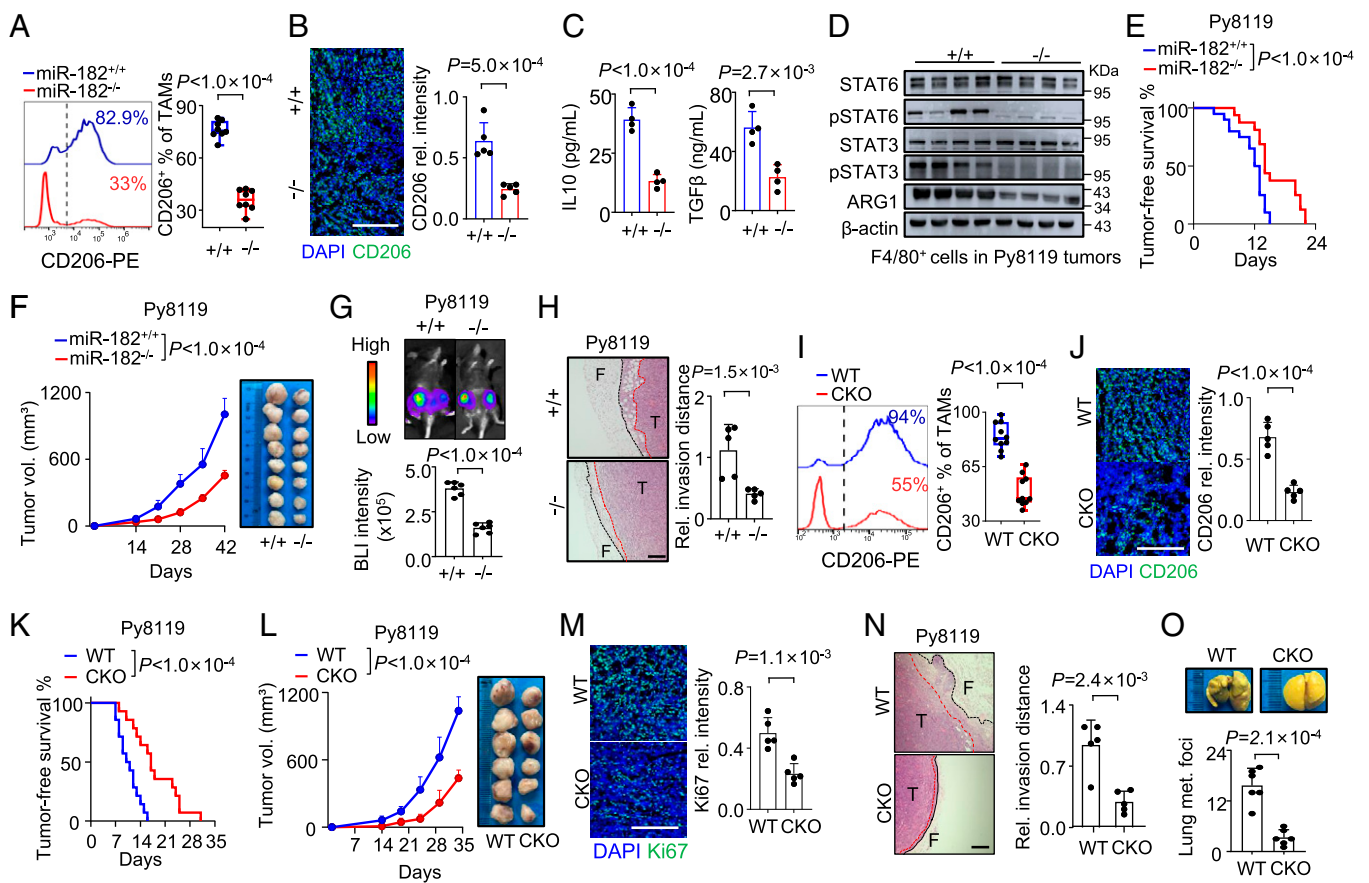
Fig. 2. miR-182 deletion in host mice and macrophages suppresses M2 polarization and tumor development. (*A–H*) Analyses of macrophage polarization and tumor progression in miR-182-KO (miR-182^{−/−}, [−/−]) or wild-type (miR-182^{+/+}, [+/+]) mice with orthotopic injection of Py8119 cells. Shown are flow cytometric analysis of the CD206^{+} percentage of F4/80^{+}CD11b^{+} macrophages in Py8119 tumors (*A*, n = 8 tumors each group), CD206 staining of the tumors (*B*, n = 5 tumors each group), ELISA of serological IL10 and TGFβ of the mice (*C*, n = 4 mice each group), ARG1 expression and STAT3/6 phosphorylation in F4/80^{+} cells of the tumors (*D*), tumor initiation analysis by tumor-free survival curves (*E*, n = 16 and 20 tumors for KO and wild-type groups), tumor growth (*F*, n = 14 tumors from 7 mice each group), bioluminescent imaging (BLI) of tumor burden 6 wk after Py8119 injection (*G*, n = 6 mice each group), and tumor invasion distance from tumor edges (red dotted line) to invasive fronts (black dotted line) (*H*, n = 5 tumors each group. (*I–O*) Analyses of macrophage polarization and tumor progression in conditional miR-182-KO (CKO, miR-182^{fl/fl};*Lyz2*[cre]) or wild-type control (WT, *Lyz2*[cre]) mice with orthotopic injection of Py8119 cells. Shown are flow cytometric analysis of CD206^{+} percentage of macrophages in the tumors (*I*, n = 10 mice each group), CD206 staining of the tumors (*J*, n = 5 tumors each group), tumor initiation analysis by tumor-free survival curves (*K*, n = 14 tumors from 7 mice each group), tumor growth (*L*, n = 14 tumors from 7 mice each group), Ki67 analyses of the tumors (*M*, n = 5 tumors each group), tumor invasion distance from tumor edges to invasive fronts (*N*, n = 5 tumors each group, and numbers of pulmonary nodules (*O*, n = 6 mice each group). (Scale bar, 100 μm.) P values were obtained by two-tailed unpaired t test (*A–C*, *G–J*, and *M–O*), log-rank test (*E* and *K*) or two-way ANOVA (*F* and *L*). Box plots display values of minimum, first quartile, median, third quartile, and maximum (*A* and *I*). Bar graphs show mean + SD (*B–D*, *G*, *H*, *J*, and *M–O*). Data points show mean + SEM (*F* and *L*).

or GCSF, were reduced in KO mice (Fig. 2*C* and *SI Appendix*, Fig. S2*B*). Suppression of STAT3 and STAT6 phosphorylation as well as ARG1 and *Il10* expression was also observed in the macrophages of tumors transplanted in KO mice (Fig. 2*D* and *SI Appendix*, Fig. S2*C*). miR-182 deficiency in host mice also suppressed the initiation, growth, and metastasis of transplanted tumors (Fig. 2 *E–H* and *SI Appendix*, Fig. S2 *D and E*). Together with the reduction of M2 macrophages in the tumors of miR-182-KO mice, we also observed a decrease of CD4^{+} T cell population and an increase of CD8^{+} T cell population in these tumors, which is concordant to the immune-suppressive role of M2 macrophages (*SI Appendix*, Fig. S2 *F and G*). The abundance of myeloid-derived suppressor cells and B cells was not obviously changed (*SI Appendix*, Fig. S2 *H and I*).

We repeated the transplanting experiments with orthotopic injection of AT3 breast cancer cells into wild-type and KO mice and observed similar phenomena in M2 macrophages and tumor development (*SI Appendix*, Fig. S2 *J–N*). These data demonstrated a role of miR-182 in tumor microenvironment for TAM polarization and tumor development.

To further assess the function of miR-182 in macrophages, we generated a conditional miR-182-KO mouse model by flanking the miR-182 gene with LoxP sites (*SI Appendix*, Fig. S2*O*). Crossing the mice with the strain harboring lysozyme 2-driven Cre recombinase (*Lyz2*[cre]) resulted in specific deletion of miR-182 in monocytes (*SI Appendix*, Fig. S2 *O and P*). Then, Py8119 cells were transplanted into the mammary fat pads of the mice. Concordant to the observations in constitutive KO mice, miR-182 deletion in monocytes did not affect the abundance of total macrophages in breast tumors (*SI Appendix*, Fig. S2*Q*) but led to a reduction of M2 fraction and an elevation of iNOS^{+} M1 fraction of macrophages (Fig. 2 *I and J* and *SI Appendix*, Fig. S2*R*). In addition, fewer CD4^{+} T cells and more CD8^{+} T cells were observed in the tumors of conditional KO mice (*SI Appendix*, Fig. S2*S*). Accompanied with these changes was the inhibition of tumor initiation and progression (Fig. 2 *K–O*). Thus, miR-182 deletion in macrophages also resulted in deficiency of TAM polarization and tumor development.

miR-182 Promotes M2 Polarization of Macrophages In Vitro. To validate the effect of miR-182 in macrophage activation, bone marrow cells were isolated from wild-type or miR-182-KO mice, followed by treatment with macrophage colony stimulating factor (M-CSF) for macrophage differentiation. Consistent with the observations in mice, miR-182 deficiency led to no obvious changes in macrophage differentiation (*SI Appendix*, Fig. S3*A*). However, when the bone marrow-derived macrophages (BMDMs) were further activated by IL4 and IL13, miR-182 deficiency significantly weakened the tendency of BMDMs to activate into CD206^{+} M2 macrophages (Fig. 3 *A and B*). Secretion of IL10 and TGFβ was also reduced in the miR-182-deficient macrophages (Fig. 3*C*). qPCR of additional M2 marker genes, including *Arg1*, *Chia1*, *Clec7*, *Dgat1*, and *Jag1*, also confirmed the conclusion (Fig. 3*D*). Furthermore, when Py8119 cancer cells were cultured with the conditioned media of BMDMs, cancer cell proliferation and tumorsphere formation were weakened in the media of miR-182-deficient BMDMs as compared to those of normal BMDMs (*SI Appendix*, Fig. S3 *B and C*).

Then, miR-182 was overexpressed with a microRNA mimic in THP1 and U937 cells (*SI Appendix*, Fig. S3*D*), followed by phorbol-12-myristate-13-acetate (PMA) and IL4/13 treatment of the cells for M2 macrophage differentiation (*SI Appendix*, Fig. S3*E*). miR-182 overexpression obviously promoted the expression of CD163, CD206, IL10, and additional M2 markers in both THP1 and U937 (Fig. 3 *E and F* and *SI Appendix*, Fig. S3*F*). STAT3/6 phosphorylation as well as ARG1 expression were also enhanced by miR-182 overexpression in macrophages (Fig. 3*G*).
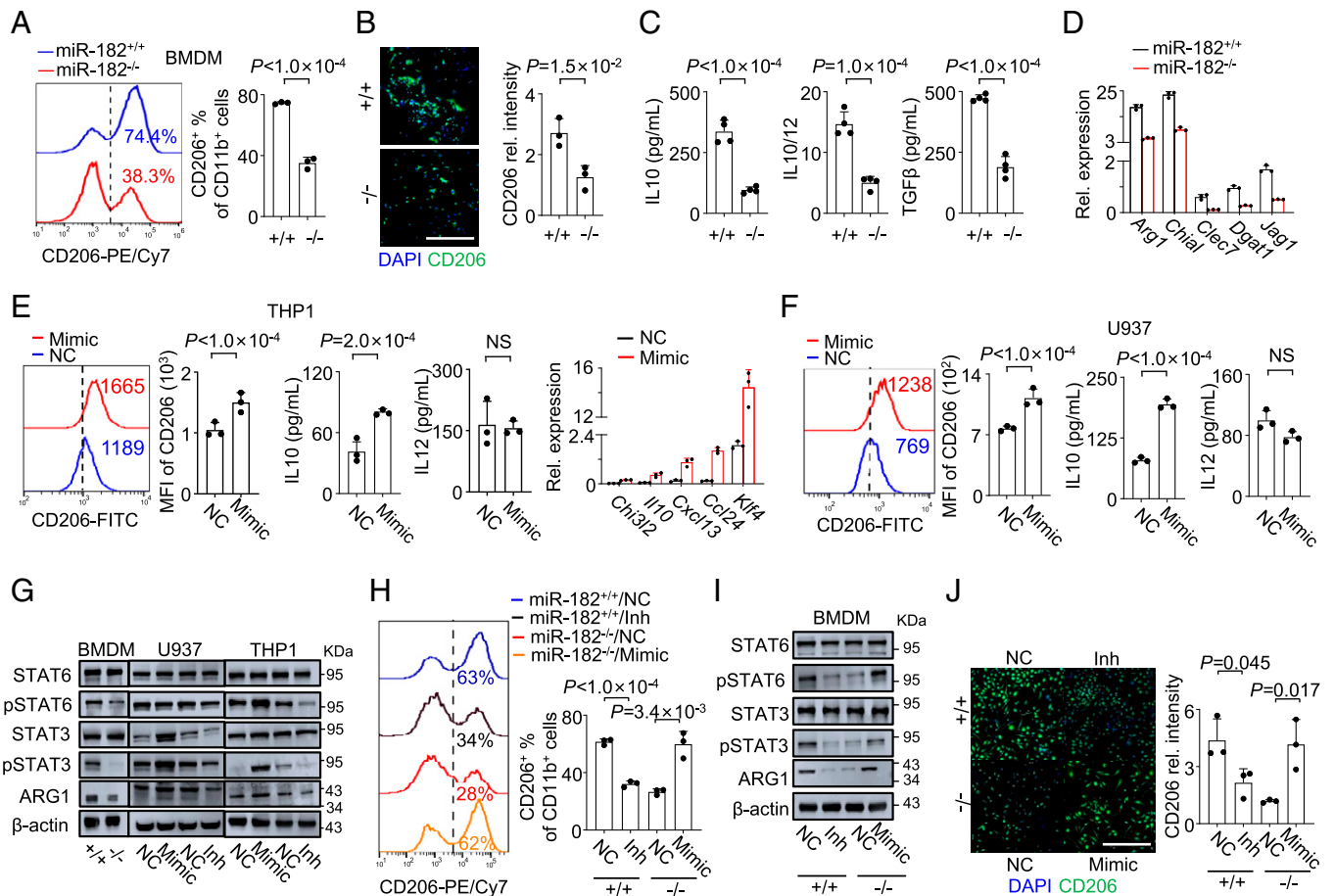
Notably, miR-182 overexpression also promoted the capacity of macrophage conditioned media to facilitate breast cancer cells for tumorsphere formation (*SI Appendix*, Fig. S3*G*) and escaping T cell cytotoxicity (*SI Appendix*, Fig. S3 *H–J*).

Reciprocally, when miR-182 was knocked down with an oligonucleotide inhibitor in THP1 and wild-type BMDMs (*SI Appendix*, Fig. S3*D*), M2 polarization was depressed (Fig. 3 *G–J*), a phenomenon similar in miR-182-KO BMDMs. More importantly, re-expression of miR-182 in the miR-182-KO BMDMs by the miR-182 mimic rescued the effect of miR-182 depletion and recovered M2 polarization (Fig. 3 *H–J*). Taken together, our data confirmed the role of miR-182 in macrophages to promote M2 polarization and facilitate tumor progression.

Macrophage Regulation Mediates the Effects of miR-182 in Tumor Progression. As previous studies have shown that miR-182 could regulate autonomous behaviors of cancer cells, we further used several animal assays to test whether the observed effects of miR-182-KO in breast cancer in our study are dependent on macrophage regulation. First, clodronate liposome was used to deplete macrophages in wild-type or miR-182-KO mice with Py8119 tumors (*SI Appendix*, Fig. S4*A*). We found that systemic macrophage depletion abolished the differences in tumor development caused by miR-182 constitutive KO in mice. The tumors initiated and grew at similar rates in wild-type and miR-182-KO mice after clodronate treatment (Fig. 4 *A–C*). Second, Py8119 breast cancer cells and wild-type or miR-182-KO BMDMs were coinjected into the mammary glands of mice whose endogenous macrophages in mammary glands were previously depleted via combination of systemic half-lethal dose irradiation and fat-pad injection of clodronate liposome (*SI Appendix*, Fig. S4 *B and C*). Interestingly, initiation and growth of the Py8119 tumors were obviously slower with coinjection of miR-182-KO macrophages than those with wild-type macrophages in the same mice (Fig. 4 *D–F*). Tumor cell proliferation was also suppressed with miR-182-KO BMDMs (Fig. 4*G*). Third, we used a mouse model of bone marrow transplantation. Wild-type host mice irradiated at lethal dose received transplantation of bone marrow from wild-type or miR-182-KO donor mice, followed by orthotopic injection of Py8119 cancer cells (*SI Appendix*, Fig. S4 *D and E*). In the hosts reconstituted with miR-182-KO bone marrow cells, M2 polarization of the macrophages in Py8119 tumors was significantly more weakened than those in the mice with wild-type marrow transplantation (Fig. 4 *H and I*), leading to delay of tumor initiation and decrease of tumor growth and proliferation (Fig. 4 *J–L*). Overall, these data suggested that the effect of miR-182 depletion on tumor development is largely dependent on the regulation of macrophages.

Tumor Cells Induce miR-182 Expression of Macrophages by TGFβ Signaling. Next, we interrogated whether miR-182 mediates the induction of macrophage polarization by tumor cells. Culturing BMDMs in conditioned medium of Py8119 indeed induced M2 polarization of the macrophages (Fig. 5*A*). Interestingly, the expression of miR-182 in macrophages was also induced by cancer cell conditioned medium (Fig. 5*B* and *SI Appendix*, Fig. S5*A*). Notably, miR-182 expression in other immune cell types, including neutrophils and T cells, was significantly weaker than in macrophages and was not responsive to cancer cell conditioned medium (*SI Appendix*, Fig. S5*A*). In addition, the up-regulation of macrophage miR-182 was only observed in wild-type, but not miR-182-KO, macrophages when cultured in cancer cell conditioned medium (Fig. 5*C*), indicating the induction of endogenous miR-182 rather than the engulfment of exogenous miR-182 molecules in macrophages.

Then, we asked how cancer cells affect the expression of miR-182 in macrophages. Previously, we and others have
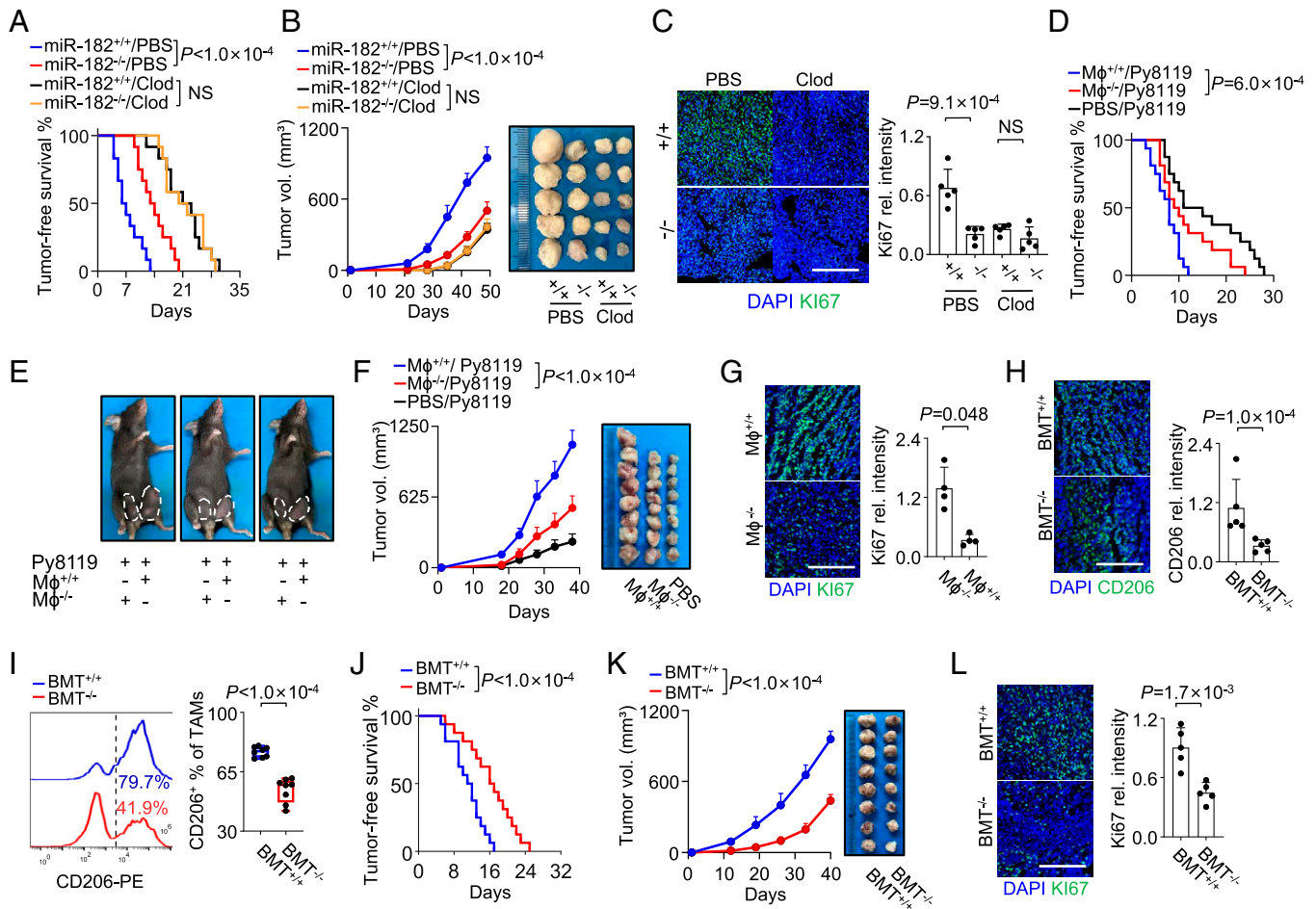
Ma et al.
miR-182 targeting reprograms tumor-associated macrophages and
limits breast cancer progression

Fig. 3. miR-182 promotes M2 polarization of macrophages in vitro. (*A–D*) Analyses of M2 polarization of wild-type ($^{+/+}$) or miR-182-KO ($^{-/-}$) BMDMs after IL4 and IL13 treatment. Shown are CD206 flow cytometry (*A*, $n = 3$ independent experiments), CD206 IF analysis (*B*, $n = 3$ independent experiments), ELISA of IL-10, TGFβ, and IL10/IL-12 ratio (*C*, $n = 4$ independent experiments), and qPCR analyses of additional M2 markers (*D*, $n = 3$ independent experiments). (*E*) Effects of miR-182 mimic on M2 polarization of THP1 macrophages after IL4 and IL13 treatment. Shown are CD206 flow cytometry, ELISA of IL10 and IL10/IL12 ratio, and qPCR analyses of additional M2 markers ($n = 3$ independent experiments). NC, negative control. (*F*) Effects of miR-182 mimic on M2 polarization of U937-macrophages after IL4 and IL13 treatment. Shown are CD206 flow cytometry, ELISA of IL10 and IL12 secretion, and qPCR analyses of additional M2 markers ($n = 3$ independent experiments). (*G*) ARG1 protein expression and STAT3/6 phosphorylation in wild-type or miR-182-KO BMDMs and in THP1- or U937-derived macrophages treated with miR-182-overexpressing mimic or miR-182 oligonucleotide inhibitor (Inh). (*H–J*) Analysis of M2 polarization of IL4/IL13-activated wild-type BMDMs after treatment of miR-182 inhibitor (Inh) and miR-182-KO BMDMs after miR-182 overexpression. Shown are CD206 flow cytometry (*H*, $n = 3$ independent experiments), ARG1 protein expression and STAT3/6 phosphorylation (*I*), and CD206 IF analysis (*J*, $n = 3$ independent experiments). (Scale bar, 100 μm.) P values were obtained by two-tailed unpaired t test. Bar graphs show mean + SD.

reported that TGFβ could up-regulate the expression of miR-182 in glioma cells and breast cancer cells by activing the promoter activity of miR-182 in a SMAD-dependent manner (35, 46). In addition, we observed an obvious positive correlation of TGFβ expression and M2 macrophage infiltration in human breast tumors (*SI Appendix*, Fig. S5*B*). Therefore, we tested whether cancer cells induce macrophage miR-182 expression by TGFβ. We found that Py8119 and SCP28 cancer cells indeed secreted TGFβ into the conditioned medium (*SI Appendix*, Fig. S5*C*). Importantly, administration of the TGFβ inhibitor SB431542 or TGFβ neutralizing antibody (57) blocked the effect of Py8119 conditioned medium on miR-182 induction and M2 polarization of BMDMs (Fig. 5 *A* and *B* and *SI Appendix*, Fig. S5*D*). A similar phenomenon was observed when the expression of TGFβ in Py8119 was suppressed by short hairpin RNAs (shRNAs; *SI Appendix*, Fig. S5*E* and Fig. 5*D*). We also obtained the same results by treating THP1 macrophages with SCP28 conditioned medium (*SI Appendix*, Fig. S5 *F* and *G*). Further analyses showed that TGFβ could enhance the activity of miR-182 promoter (*SI Appendix*, Fig. S5*H*) and induce the expression of miR-182 in a variety of macrophage cells, including

THP1, U937, BMDMs, and RAW264.7, in a dose- and time-dependent manner (Fig. 5*E* and *SI Appendix*, Fig. S5*I*).

In addition, TGFβ treatment induced M2 polarization of wild-type BMDMs (Fig. 5 *F–H*). However, when miR-182 was knocked out or inhibited in BMDMs, BMDMs were much less responsive to TGFβ for M2 activation (Fig. 5 *F–H* and *SI Appendix*, Fig. S5*J*). Similarly, THP1- and U937-derived macrophages could also be induced to express M2 markers by TGFβ and miR-182 overexpression, while miR-182 inhibition hindered their responsiveness to TGFβ (Fig. 5 *I–K* and *SI Appendix*, Fig. S5*K*). Thus, our data support the conclusion that the secretion of TGFβ by tumor cells promotes the expression of miR-182 in macrophages, thereby inducing the polarization of macrophages to M2.

miR-182 Targets Toll-Like Receptor 4 to Regulate M2 Polarization of TAMs. We further aimed to delineate the downstream mechanism of miR-182 in macrophages for M2 regulation. The transcriptomic profiles of wild-type and miR-182-KO BMDMs were compared by RNA sequencing. Gene Ontology analysis showed that the top-up-regulated genes by miR-182-KO were mostly
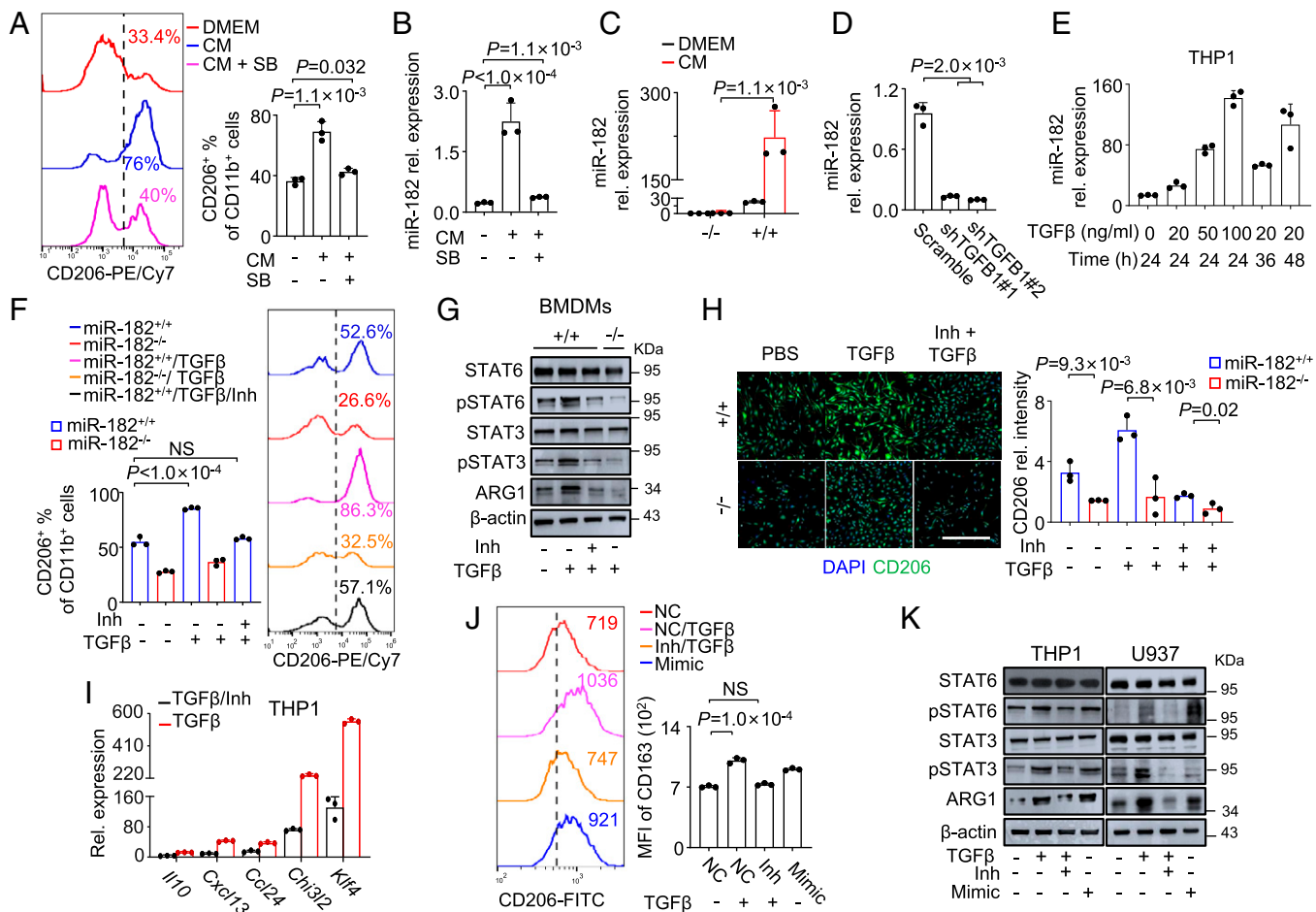
Ma et al.
miR-182 targeting reprograms tumor-associated macrophages and
limits breast cancer progression

PNAS | 5 of 12
https://doi.org/10.1073/pnas.2114006119

Fig. 4. Macrophage regulation mediates the effects of miR-182 in tumor progression. (*A–C*) Tumor development and proliferation in miR-182-KO and wild-type mice treated with clodronate liposomes (Clod) or PBS liposomes (PBS) after orthotopic injection of Py8119 cells. Shown are tumor initiation analysis by tumor-free survival curves (*A*, n = 12 tumors from 6 mice each group), tumor growth (*B*, n = 12 tumors from 6 mice each group), and Ki67 IF analysis of the tumors (*C*, n = 5 tumors each group). (*D–G*) Tumor development and proliferation in C57BL/6 mice with depletion of endogenous macrophages and coinjection of Py8119 with wild-type (Mϕ$^{+/+}$) or miR-182-KO (Mϕ$^{−/−}$) BMDMs. Shown are tumor initiation analysis by tumor-free survival curves (*D*, n = 16 tumors from 8 mice each group), representative images of tumor-bearing mice (*E*), tumor growth (*F*, n = 16 tumors from 8 mice each group), and Ki67 IF analysis of the tumors (*G*, n = 4 tumors each group). (*H–L*) Analyses of macrophage polarization and tumor progression in irradiated mice with transplantation of wild-type (BMT$^{+/+}$) or miR-182-KO (BMT$^{−/−}$) bone marrow and orthotopic injection of Py8119 cells. Shown are CD206 IF analysis of the tumors (*H*, n = 5 tumors each group), CD206 flow cytometry (*I*, n = 8 tumors each group), tumor initiation analysis by tumor-free survival curves (*J*, n =16 tumors from 8 mice each group), tumor growth (*K*, n = 16 tumors from 8 mice each group), and Ki67 IF analysis of the tumors (*L*, n = 5 tumor each group). (Scale bar, 100 μm.) *P* values were obtained by log-rank test (*A*, *D*, and *J*), two-way ANOVA (*B*, *F*, and *K*), or two-tailed unpaired *t* test (*C*, *G–I*, and *L*). Bar graphs show mean + SD (*C*, *G*, *H*, and *L*). Data points show mean + SEM (*B*, *F*, and *K*). Box plots display values of minimum, first quartile, median, third quartile, and maximum (*I*).

involved in Toll-like receptor (TLR) and its downstream NFκB signaling pathways (*SI Appendix*, Fig. S6A). Gene set enrichment analysis (GSEA) analyses also showed the up-regulation of several TLR and NFκB-related gene sets (58, 59) in miR-182-KO BMDMs (Fig. 6A). An overlapped analysis of Target-Scan (60) predicted target genes of miR-182 and KEGG (61) TLR pathway genes revealed nine candidates (*SI Appendix*, Datasets S1–S3 and Fig. S6B), among which TLR4 was of particular interest, as it is known to play a key role in macrophage polarization (62) and also reported to be a target gene of miR-182 (63). We confirmed the regulation of TLR4 by miR-182. The 3′UTR of *TLR4* contained two predicted binding sites of miR-182 (*SI Appendix*, Fig. S6C). Luciferase reporter assays showed that miR-182 mimic dose-dependently suppressed *TLR4* 3′UTR activity (Fig. 6B). When the second miR-182 binding site at *TLR4* 3′UTR was mutated (*SI Appendix*, Fig. S6C), the 3′UTR activity was no longer affected by miR-182 (Fig. 6C). More importantly, although the *TLR4* mRNA

was not affected by miR-182 (*SI Appendix*, Fig. S6D), miR-182 overexpression significantly suppressed, while its knockdown enhanced, the endogenous protein level of TLR4 in both BMDMs and THP1 macrophages (Fig. 6 *D* and *E*).

TLR4 is a member of the TLR family and known to polarize macrophages toward a proinflammatory phenotype by activating downstream MYD88-dependent NFκB signaling (64, 65). Accordingly, down-regulation of MYD88, p65 phosphorylation, and the NFκB downstream gene *Nfkbia* were observed together with miR-182 and TGFβ-induced TLR4 suppression in THP1 and BMDMs (Fig. 6 *D* and *E* and *SI Appendix*, Fig. S6 *F* and *G*). Reciprocally, miR-182-KO resulted in up-regulation of TLR4, MYD88, and p65 phosphorylation in the macrophages of breast tumors (Fig. 6F). We further knocked down *TLR4* by small interfering RNAs (siRNAs) in miR-182-KO BMDMs (Fig. 6G). *TLR4* knockdown inhibited downstream MYD88 expression and NFκB activation (Fig. 6G and *SI Appendix*, Fig. S6F) and, more importantly, led to up-regulation of M2

Ma et al.
miR-182 targeting reprograms tumor-associated macrophages and
limits breast cancer progression

Fig. 5. Tumor cells enhance miR-182 expression of macrophages by secreting TGFβ. (*A* and *B*) CD206$^+$ percentage (*A*) and miR-182 expression (*B*) of BMDMs cultured in control DMEM or Py8119 conditioned medium (CM) and treated with SB431542 (SB); $n = 3$ independent experiments. (*C*) miR-182 expression in wild-type ($^{+/+}$) or miR-182-KO ($^{-/-}$) BMDMs after treatment of Py8119 CM ($n = 3$ independent experiments). (*D*) miR-182 expression of BMDMs after treatment of CM from Py8119 cells with TGFβ knockdown ($n = 3$ independent experiments). (*E*) miR-182 expression of THP-1 macrophages after treatment of TGFβ at different concentrations for different durations ($n = 3$ independent experiments). (*F–H*) CD206 flow cytometry (*F*, $n = 3$ independent experiments), ARG1 expression and STAT3/6 phosphorylation (*G*), and CD206 IF analyses (*H*, $n = 3$ independent experiments) of wild-type or miR-182-KO BMDMs with treatment of TGFβ (50 ng/mL, 36 h) and/or miR-182 inhibitor (Inh). (*I*) Expression of M2 markers in THP1 macrophages after treatment of TGFβ (50 ng/mL, 48 h) and/or miR-182 inhibitor ($n = 3$ independent experiments). (*J*) CD206 flow cytometry of THP1 macrophages with treatment of TGFβ (50 ng/mL, 36 h), miR-182 mimic or inhibitor ($n = 3$ independent experiments). NC, negative control. (*K*) ARG1 expression and STAT3/6 phosphorylation of THP1 and U937 macrophages with treatment of TGFβ (50 ng/mL, 36 h), miR-182 mimic, or inhibitor. (Scale bar, 100 μm.) P values were obtained by two-tailed unpaired t test. Bar graphs show mean + SD.

markers (Fig. 6 *H–J*). *TLR4* knockdown rescued the effect of miR-182 deficiency on macrophage polarization (Fig. 6 *I* and *J*). Reciprocally, stable overexpression of *TLR4* in THP1 (*SI Appendix*, Fig. S6*E* and Fig. 6*G*) obviously repressed NFκB activation and M2 polarization (*SI Appendix*, Fig. S6*F* and Fig. 6 *H* and *K*). In addition, the suppression of CD206 and CD163 expression by *TLR4* overexpression was diminished by miR-182 overexpression (Fig. 6*K* and *SI Appendix*, Fig. S6*H*). These data demonstrated that miR-182 directly targets TLR4 in macrophages to suppress NFκB and promote M2 polarization.

AntagomiR Targeting miR-182 in Macrophages Suppresses Tumor Development. The essential function of miR-182 in TAMs implies that it is a potential target for cancer therapy. Thus, we designed an antagomiR inhibitor of miR-182 and adopted a recently reported macrophage-targeting "eat me" strategy with cationized mannan-modified extracellular vesicles (M-EVs) (66, 67) for in vivo delivery of the inhibitor into TAMs. Extracellular vesicles (EVs) were isolated from mesenchymal stem cells (MSCs; *SI Appendix*, Fig. S7*A*) and modified with

cationized mannan, which is the ligand of the surface receptor CD206 (also called MRC1) expressed by M2 macrophages, followed by electroporation loading of the antagomiR-182 inhibitor (Fig. 7*A*). The macrophage-targeting efficiency of the cationized M-EVs was first confirmed, as they were internalized by macrophages with much higher efficiency than by tumor cells (Fig. 7 *B* and *C*). M-EV loading of antagomiR-182 resulted in a striking improvement of miR-182 inhibition in macrophages, but not in tumor cells, as compared to the unpackaged inhibitor (Fig. 7*D*). M-EV delivery also enhanced the efficiency of antagomiR-182 to inhibit M2 polarization of macrophages in vitro (Fig. 7*E*).

Then, we assessed the efficiency of antagomiR-182 delivered in M-EVs for cancer therapy in vivo. Py8119 cells were orthotopically injected into C57BL/6 mice, followed by intratumoral injection of the antagomiR-182-loaded M-EVs every 5 d (*SI Appendix*, Fig. S7*B*). A test with dye-labeled M-EVs showed that the vesicles were mainly distributed in the injected mammary glands without obvious spreading to other organs of the mice (*SI Appendix*, Fig. S7*C*). Importantly, antagomiR-182
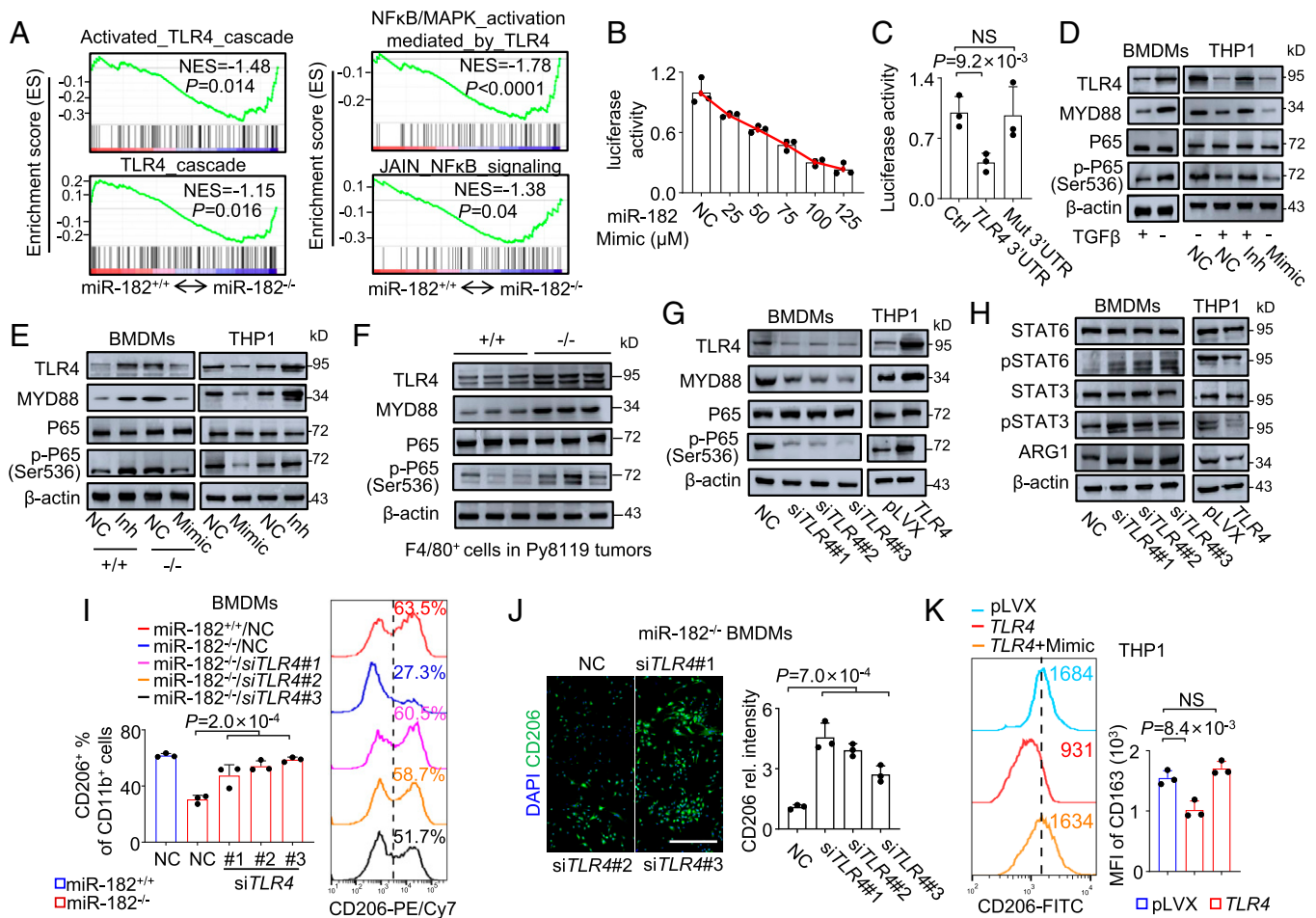
Fig. 6. miR-182 regulates macrophage polarization by targeting TLR4. (*A*) GSEA analyses of TLR4 and NFκB pathway gene sets in breast tumors from PyMT;miR-182^{+/+} vs. MMTV-PyMT;miR-182^{−/−} mice. (*B*) *TLR4* 3′UTR luciferase activity after transfection of various amount of miR-182 mimic in HeLa (*n* = 3 independent experiments). (*C*) Luciferase activities of wild-type and mutated *TLR4* 3′UTR after transfection of miR-182 mimic (100 μM) in HeLa (*n* = 3 independent experiments). (*D*) TLR4 and MYD88 expression and P65 phosphorylation in BMDMs, and THP1 macrophages after treatment of TGFβ and/or miR-182 mimic or inhibitor. (*E*) TLR4 and MYD88 expression and P65 phosphorylation in wild-type ([+/+]) or miR-182-KO ([−/−]) BMDMs, and THP1 macrophages after treatment of miR-182 mimic or inhibitor. (*F*) TLR4 and MYD88 expression and P65 phosphorylation in F4/80^{+} cells of Py8119 tumors in wild-type or miR-182-KO mice. (*G*) TLR4 and MYD88 expression and P65 phosphorylation in BMDMs with *TLR4* knockdown and THP1 macrophages with *TLR4* overexpression. (*H*) ARG1 expression and STAT3/6 phosphorylation in BMDMs with *TLR4* knockdown and THP1 macrophages with *TLR4* overexpression. (*I*) CD206 flow cytometry in wild-type or miR-182-KO BMDMs with *TLR4* knockdown (*n* = 3 independent experiments). (*J*) CD206 IF analyses of miR-182-KO BMDMs with *TLR4* knockdown (*n* = 3 independent experiments). (*K*) CD206 flow cytometry of THP1 macrophages with treatment of miR-182 mimic and/ or *TLR4* overexpression (*n* = 3 independent experiments). (Scale bar, 100 μm.) *P* values were obtained by two-tailed unpaired *t* test (*C* and *I*–*K*). Bar graphs show mean + SD.

delivered by M-EVs showed no obvious toxicity in the mice (*SI Appendix*, Fig. S7D). The treatment effectively suppressed the expression of miR-182 both in F4/80[+] and F4/80^{−} cells of Py8119 tumors but with the inhibiting efficiency obviously higher in F4/80^{+} cells (*SI Appendix*, Fig. S7E). TLR4 was significantly enhanced in F4/80^{+} cells by the treatment (*SI Appendix*, Fig. S7F). It was found that the treatment did not change the total abundance of macrophages in tumors (*SI Appendix*, Fig. S7G) but significantly suppressed M2 polarization of TAMs (Fig. 7F). Consequently, miR-182 targeting in macrophages resulted in obvious suppression of tumor growth and lung metastasis (Fig. 7 *G* and *H* and *SI Appendix*, Fig. S7H). The tumors in the same mice were halted by the miR-182 inhibitor but not by the empty M-EVs (Fig. 7G). We repeated the therapeutic testing of antagomiR-182 delivery to treat 4T1 orthotopic tumors in BALB/c mice and again observed effective suppression of M2 macrophages and tumor growth (Fig. 7 *F–H*, and *SI Appendix*, Fig. S7I). These data corroborate the potential of miR-182 inhibition for TAM-targeting therapy in breast cancer.

Discussion

Recently, miR-182 has emerged as an important regulator of cancer. It has been widely observed as one of the top up-regulated microRNAs in tumor tissues (17–24, 34, 49) and plays promoting roles in tumorigenesis and metastasis of breast cancer, lung cancer, glioma, melanoma, and ovarian cancer (16, 26–36, 38, 39, 41, 42, 49). However, previous analyses of miR-182 in cancer are mainly performed in cancer cell lines, and studies with genetic mouse models are lacking. In addition, the expression dysregulation and functional influence of miR-182 in cancer may not be limited to tumor cells. In this study, we first used a constitutive miR-182-KO mouse model to confirm the critical role of the microRNA in tumor development and further showed that miR-182 genetic deficiency in tumor host tissues and, more specifically, in macrophages deprived tumors of M2-like TAMs, leading to repression of tumor development. Mechanistic studies revealed miR-182 as a mediator for tumor education of macrophages by responding to tumor-derived TGFβ and regulating the TLR4/NFκB signaling to drive TAM
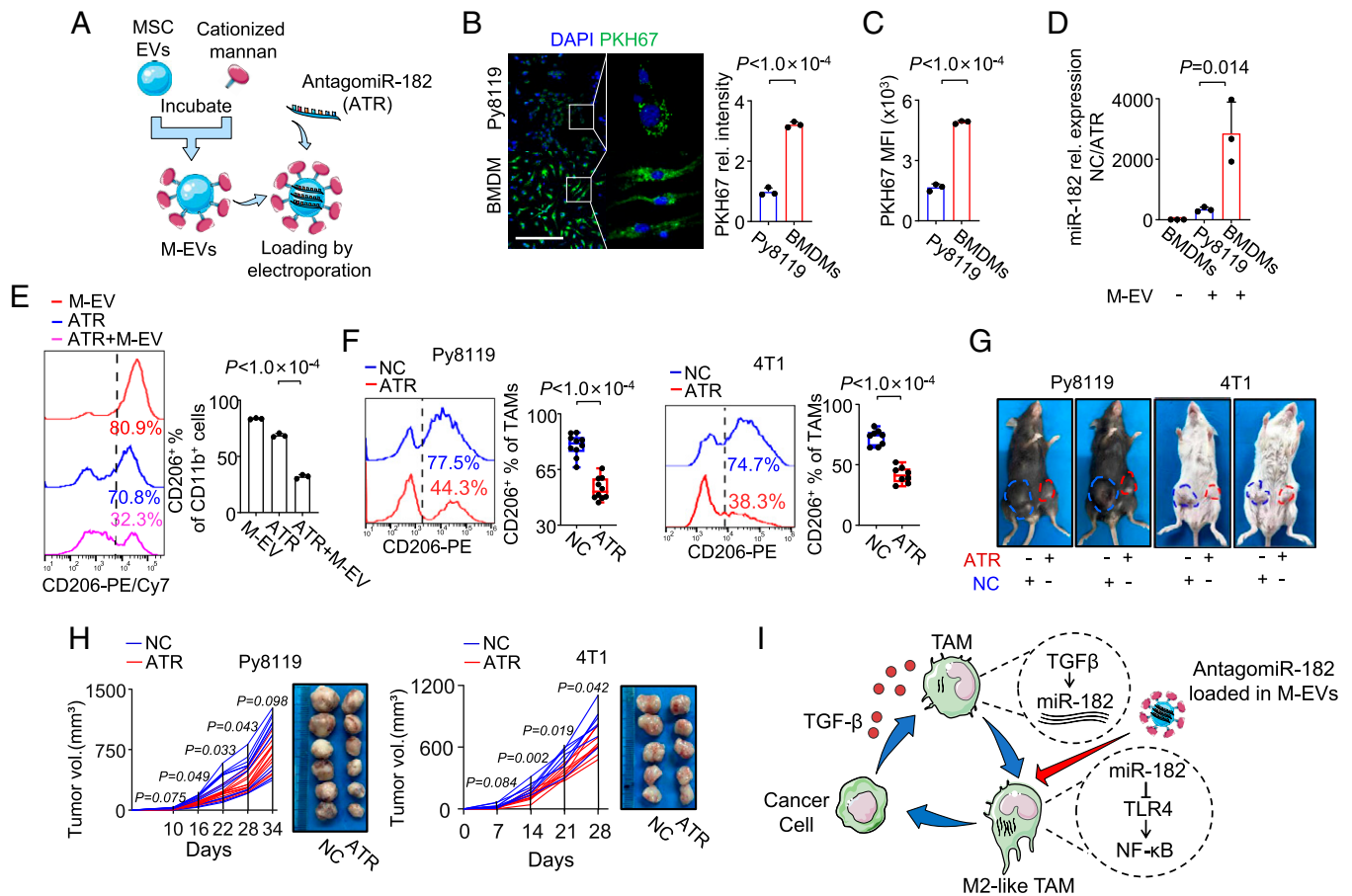
Fig. 7. Macrophage targeting with M-EV delivery of antagomiR-182 suppresses tumor development. (*A*) Schematic of the process for preparation of cationized mannan-modified EVs (M-EVs) and antagomiR-182 (ATR) loading. (*B* and *C*) Internalization efficiency of PKH67-labeled M-EVs by BMDMs or Py8119, as shown by PKH67 IF analysis (*B*) and flow cytometry (*C*); *n* = 3 independent experiments. (*D*) miR-182 knockdown efficiency in BMDMs or Py8119 cells after treatment of naked or M-EV-loaded antagomiR-182; *n* = 3 independent experiments. (*E*) CD206 flow cytometry of BMDMs treated with empty M-EVs, naked (ATR) or M-EV-loaded antagomiR-182 (ATR+M-EV); *n* = 3 independent experiments. (*F*–*H*) Macrophage polarization and tumor development in mice with orthotopic injection of Py8119 or 4T1 cells and treatment of M-EV-loaded antagomiR-182. Shown are CD206 flow cytometry of the F4/80$^+$CD11b$^+$ macrophages in transplanted tumors (*F*, *n* = 10 mice each Py8119 group; *n* = 8 mice each 4T1 group), representative images of mice with treated and untreated tumors on each side (*G*), and tumor growth curves (*H*, *n* = 12 tumors each Py8119 group; *n* = 8 tumors each 4T1 group). (*I*) Schematic of the role of miR182 in TAM polarization. (Scale bar, 100 μm.) *P* values were obtained by two-tailed unpaired *t* test. Bar graphs mean + SD. Data points show mean + SEM. Box plots display values of minimum, first quartile, median, third quartile, and maximum (*F*).

polarization (Fig. 7*I*). Our study of miR-182 in TAMs is largely consistent with a previous study reporting that miR-182 regulates TLR4 in macrophages to alleviate inflammation in myocardial infarction (63). However, our data do not exclude the previously validated role of miR-182 in cancer cells. In addition, the involvement of miR-182 in tumor microenvironment might even go beyond macrophages. For example, we also found the up-regulation of miR-182 expression in tumor-associated fibroblasts as compared to normal fibroblasts (*SI Appendix*, Fig. S7*J*). miR-182 is also the most induced miRNA in B cells undergoing class-switch recombination (68, 69). In addition, miR-182 could also induce regulatory T cell differentiation (44, 70). Thus, miR-182 might play versatile roles in cancer cells and tumor microenvironment. As multiple cancer types are known to secret TGFβ abundantly and thus could regulate microenvironmental miR-182 expression, the microenvironmental role of miR-182 and its therapeutic potential are unlikely to be limited to breast cancer, although our study mainly focuses on breast cancer. Nevertheless, our study will expand the understanding of the involvement of miR-182 in cancer and support the rationale of miR-182 targeting for cancer treatment.

Although both our study and the previous report (63) showed that miR-182 directly targets TLR4 and suppresses the downstream NFκB signaling to regulate macrophage polarization, we also noticed that *TLR4* suppression by some siRNA inhibitors cannot completely restore the phenotype caused by miR-182-KO, indicating TLR4 may not be the only downstream factor participating in this process. Our previous study reported that miR-182 regulates the accumulation of triglyceride in cancer cells (49), while lipid metabolism has been known to be critical for macrophage polarization (71–73). In addition, HIF-1α signaling, which could be regulated by miR-182 (74), is also known to be critical for alternative activation of macrophages (71). Therefore, the role of miR-182 in macrophage modulation is worthy of further investigation, and the possibility of mechanisms other than TLR4 should not be excluded.

Since TAMs play important roles in tumor initiation, growth, and metastasis, unraveling the crucial regulators of macrophage polarization in tumor microenvironment may bring opportunities in cancer therapy. Indeed, our findings of miR-182 in TAMs provide a potential strategy for TAM targeting and demonstrate the effectiveness of miR-182-inhibiting RNA interference (RNAi) therapy. Due to its advantages, including high

targeting specificity, convenience for inhibitor designing and synthesis, and the potential to target nearly all genes of interest, RNAi therapy is a long-sought strategy for cancer treatment. However, the issues of oligonucleotide stability and drug delivery greatly limit the scope of application of siRNA drugs (75). The recently reported approach using EVs or exosomes provides a promising solution to these issues (67, 76–78). In particular, delivery with mannan-coupled EVs, taking advantage of the highly expressed CD206, the receptor of mannan, on TAMs, and the innate endocytosis capacity of macrophages, is an efficient TAM-targeting strategy (66, 67). Our data confirmed that miR-182-targeting antagomiR can be specifically delivered into macrophages in vitro and in vivo, resulting in obvious tumor suppression. In addition, this strategy might be further improved. In our study, MSC-derived EVs were used to deliver antagomiR due to the promising potential of MSC-EVs in disease therapy (79). However, other cell types could also be used for EV preparation. For example, EVs derived from dendritic cells can be more readily accumulated in macrophages and also promote immune responses of macrophages due to the presence of MHC and T cell costimulatory molecules on the surface of dendritic cell EVs (67).

Overall, our study highlights a role of the miR-182/TLR4/NFκB axis for tumor-induced macrophage polarization in breast cancer. Clinical analyses demonstrate the correlation of miR-182 expression and M2-like TAM infiltration in human tumor tissues. The study also provides a promising TAM-targeting RNAi strategy for cancer therapy. Further clinical studies are needed to confirm the value of miR-182 as a potential prognostic marker and therapeutic target in cancer.

Materials and Methods

Constructs and Reagents. The miR-182 mimic, 2′methoxy modified miR-182 oligonucleotide inhibitor, *TLR4* siRNAs, and the negative control oligonucleotides were purchased from GenePharme. AntagomiR-182 and the negative control were purchased from RIBOBIO. For *TGFβ1* knockdown, shRNA sequences were obtained from the MISSION shRNA library (Sigma), then annealed and cloned into the pLKO.1-blasticidin vector (Addgene). Human *TLR4* cDNA sequence was constructed into pLVX-puro vector (Clontech) for overexpression. The +4422 to +5236 3′UTR DNA sequence flanking the transcription end site of *TLR4* was cloned into the '3 region of Renilla luciferase gene of psi-Check2 vector (Promega). For miR-182 promoter reporter assays, a 2.5-kb fragment upstream of the miR-182 gene was cloned into pGL3basic (Ambion) with NheI and XhoI digestion (35). The sequences of all oligonucleotides used in this study are provided in *SI Appendix,* Datasets S4. For Western blotting and IF analyses, the following antibodies were used: β-actin (A2228, Sigma), CD206 (187041AP, Proteintech), STAT6 (51073, Proteintech), p-STAT6 (56554S, CST), STAT3 (4904P, CST), p-STAT3 (9145P, CST), ARG1 (16001 Proteintech), TGFB1 (189781AP, Proteintech), TLR4 (sc-293072, Santa Cruz), MYD88 (4283S, CST), p-P65^{Ser536} (3033, CST), p-P65^{Ser276} (SAB4504488, Sigma), p65 (sc-372, Santa Cruz), pan-Cytokeratin (sc-8018, Santa Cruz), Alexa Fluor 488 donkey anti-rabbit IgG (A-21206, Invitrogen), HRP-conjugated goat anti-mouse IgG (401215, Merck/Millipore), and HRP-conjugated goat anti-rabbit IgG (401315, Merck/Millipore). The antibodies used for flow cytometric analyses were as follows: anti-mouse CD11b-APC (M1/70, 17011281, eBioscience), anti-mouse F4/80-PE (BM8, 12480182, eBioscience), anti-mouse CD206-PE/Cy7 (C068C2, 141719, Biolegend), anti-mouse CD206-FITC (C068C2, 141703, Biolegend), anti-human CD206-FITC (15-2, 321104, Biolegend), anti-human CD163-FITC (GHI/61, 333617, Biolegend), Alexa Fluor 700 anti-mouse CD45 (103128, Biolegend), PE/Cy7 anti-mouse CD3ε (100320, Biolegend), Pacific Blue anti-mouse CD4 (100428, Biolegend), Brilliant Violet 605 anti-mouse CD8a (100744, Biolegend), Brilliant Violet 510 anti-mouse/human CD11b (101263, Biolegend), FITC anti-mouse/human CD45R/B220 (103206, Biolegend), anti-mouse NOS2 PE (12-5920-82, Thermo Fisher Scientific), and FITC anti-mouse Ly-6G/Ly-6C (Gr-1) (108406, Biolegend). Recombinant proteins and chemicals used for in vitro assays were as follows: murine M-CSF (3150210, PeproTech), murine IL4 (AF214145, PeproTech), murine IL13 (2101310, PeproTech), recombinant mouse TGFβ1 (7666-MB-005, R&D), recombinant human TGFβ1 (240-B-002, R&D), human IL13 (2001310, Pepro-Tech), the TGFβ inhibitor SB431542 (S1067, Selleck), phorbol 12-myristate

13-acetate (P8139, Sigma), dimethyl sulfoxide (DMSO; 54686, Biomol), mannan (M7504-1G, Sigma), and N,N-carbonyldiimidazole (115533-10G, Sigma).

microRNA Detection. Total RNAs were extracted by TRIzol reagent (Invitrogen, 15596018), and mature microRNAs were reverse transcribed by TaqMan MicroRNA Reverse Transcription Kit (4366597, Invitrogen). Then, the TaqMan microRNA Assay Kit (#000597, ABI) was used to for qPCR detection. The data were normalized to U6 expression.

Luciferase Reporter Assays. For *TLR4* 3′UTR assays, HeLa cells were cotransfected with the miR-182 mimic or negative control and the psi-Check2 vector with *TLR4* 3′UTR or its mutation at the end of Renilla luciferase coding sequence. Lysates were collected 72 h after transfection. Firefly and Renilla luciferase activities were measured with Dual-Luciferase Reporter System (E1910, Promega) at 36 h posttransfection. Renilla luciferase activities were normalized with firefly luciferase activities for 3′UTR activities.

For miR-182 promoter assays, the pGL3basic vector containing the miR-182 promoter sequence was transfected into THP1-derived macrophages with Lipofectamine 3000 (L3000015, Thermo Fisher Scientific). After 48 h, TGFβ of indicated concentrations was added for stimulation. The lysates were collected, and the luciferase activity was measured after 24 h.

EV Purification and Labeling. MSC-derived EVs were isolated by differential centrifugation. Briefly, MSCs were cultured in medium containing EV-depleted fetal bovine serum (FBS) for 72 h. The supernatant of the culture was centrifuged at 2,000 *g* for 5 min and filtered using 0.2-μm filter to remove cells and debris. Next, the samples were subjected to ultracentrifugation at 10,000 *g* to deplete the microvesicles. After discarding the pellet, the supernatant was ultracentrifuged at 100,000 *g* for 70 min at 4 °C. Then, the pellet was resuspended in phosphate buffered saline (PBS) and ultracentrifuged again at 100,000 *g* for another 70 min. The precipitated vesicles were suspended in PBS carefully. EVs were either used immediately (on ice) or stored at −80 °C. PKH67 Cell Linker Kit (midi67, Sigma) was used to label EVs. EV-depleted FBS was prepared by filtering FBS with a 0.2-μm filter, followed by ultracentrifugation at 100,000 *g* overnight.

Synthesis of Cationized Mannan and Preparation of AntagomiR-182-Loaded M-EVs. The cationized mannan was synthesized as previously reported (67). Briefly, mannan (100 kDa, 20 mg) was suspended in 20 mL anhydrous DMSO. Then, spermine (748 mg) and N,N-carbonyldiimidazole (105.2 mg) were added to the mixture and kept at 35 °C for 20 h under moderate stirring. EVs modified with cationized mannan (M-EVs) were engineered by mixing the EVs isolated from MSCs with the cationized mannan. The reaction was kept at room temperature for 15 min (67). The protein concentrations of M-EVs were determined. For each injection, 2 μg M-EVs and 10 nmol of antagomiR-182 or negative control were mixed in 100 μL of electroporation buffer (1.15 mM potassium phosphate pH 7.2, 25 mM potassium chloride, 21% OptiPrep) (77) and then electroporated in a 1-mm cuvette. The liquid after electroporation was pooled for ultracentrifugation followed by resuspension in 80 μL 5% glucose.

IF Staining. The tumor tissues were fixed in 4% paraformaldehyde (PFA) for 2 h at 4 °C on a shaker, dehydrated by 20% sucrose in PBS for 4 h, then dehydrated by 30% sucrose PBS solution overnight and embedded in optimal cutting temperature compound (4583, Sakura) for 30 min at 4 °C, followed by freezing at −80 °C. Tissues were sectioned to 10 μm thickness. Sections were washed twice with PBS, permeabilized with 0.2% Triton X-100, and blocked with 3% normal donkey serum for 1 h at room temperature. Then, the sections were incubated with the primary antibody overnight at 4 °C and fluorescent-labeled secondary antibody for 1 h at room temperature, respectively. Before mounting by Dako (S3023, Agilent), nuclei were stained by DAPI (10236276001, Roche). For IF staining of cultured cells, cells were seeded on coverslips in 24-well plates, fixed with 4% PFA for 15 min, and permeated by 0.3% Triton X-100 buffer at room temperature for 10 min. Then, the staining with antibodies was performed as described previously.

FISH. The Cy3-miR-182 probe (F07101, GenePharme) and miR-182 FISH Kit (F04501, GenePharme) were used to analyze the level of miR-182 in paraffin-embedded breast tumor sections, following the manufacturer's instructions.

Flow Cytometry Analyses. Mice were euthanized at week 2 to 3 posttransplantation and tumors were harvested. Single-cell suspensions of mammary glands or tumors were prepared as described previously (80). Briefly, tissues were picked, minced, and further digested by 5 mg/mL Collagenase Type III (LS004182, Worthington), 0.001% (W/V) DNase 1 (D-4527, Sigma), and 1% (wt/wt) Dispase (17105041, Invitrogen) at 37 °C for 1 h. Cells were filtered with

a 70-μm strainer before erythrocyte lysis with the lysis buffer (555899, BD Pharmingen). FcR was blocked by a CD16/CD32 antibody (2.4G2, BD Life Sciences) at the concentration of 0.5 mg per million cells before antibody staining. Antibodies were diluted for staining according to the manufacturer's instructions. For CD206 intracellular staining, cells were fixed with IC Fixation Buffer (008222, eBioscience), permeabilized with Permeabilization Buffer (008333, eBioscience) and subsequently incubated with antibodies as described previously. Flow cytometry was performed with Gallious (Beckman) fluorescence activated cell sorting system and quantified by the FlowJo V10 software.

Enzyme-Linked Immunoassay. Enzyme-linked immunoassay (ELISA) kits were used to analyze the levels of murine IL10 (KE10008, Proteintech), murine IL12 (KE10014, Proteintech), murine TGFB1 (KE10005, Proteintech), murine GCSF (KE10025, Proteintech), human IL10 (KE00012, Proteintech), and human IL12 (KE00019, Proteintech), following the manufacturer's instructions.

Cell Culture and Macrophage Differentiation. Py8119 cell, AT3 cell, and SCP28 cell were cultured in Dulbecco's Modified Eagle Medium (DMEM) containing 10% FBS. THP1 and U937 were obtained from the Cell Bank of the Chinese Academy of Sciences. Jurkat, CTLL2, and PBMC were obtained from American Type Culture Collection (ATCC) and were cultured and activated according to the ATCC instructions (https://www.atcc.org/). All cell lines were tested as *Mycoplasma* free. Lipofectamine 2000 (11668019, Thermo Fisher Scientific) was used to transfect siRNAs, miR-182 mimic, or oligonucleotide inhibitor into BMDMs or U937-/THP1-derived macrophages. Follow-up experiments were generally carried out around 36 to 48 h after the transfection. For macrophage differentiation, bone marrow cells were cultured in 1640 containing 10% heat-inactivated FBS, and BMDMs were obtained as previously described (81). Then, BMDMs were stimulated with murine IL4 (20 ng/mL) and IL13 (20 ng/mL) for 1 to 2 d for M2 activation (81). THP1 and U937 cells were cultured in 1640 medium containing 10% heat-inactivated FBS. For macrophage differentiation, THP1 and U937 cells were stimulated with 50 ng/mL PMA for 48 h. For M2 activation, U937 or THP1-derived macrophages were further treated with human IL13 (20 ng/mL) and IL4 (25 ng/mL) for 48 h. Unless stated, the concentrations and duration of various reagents for cell culture treatment are as follows: miR-182 mimic (25 μM), miR-182 oligonucleotide inhibitor (25 μM), and TGFβ (50 ng/mL, 36 h).

Tumorsphere Formation Assays. A total of 1,000 Py8119 cells or 5,000 SCP28 cells were seeded in 6-well ultralow attachment plates (3471, Corning) in 1:1 DMEM/F-12 media supplemented with 1:50 B27 (12587010, Thermo Fisher Scientific), 20 ng/mL epidermal growth factor (PHG0311, Thermo Fisher Scientific), 10 ng/mL basic fibroblast growth factor (F0291, Sigma-Aldrich), 5 μg/mL heparin sulfate (H3149, Sigma-Aldrich), and 5 μg/mL insulin (11376497001, Roche). Spheres with diameters larger than 50 μm were counted under the microscope after 1 wk of culturing.

Mouse Experiments. All animal studies were conducted according to the guidelines for the care and use of laboratory animals and were approved by Institutional Biomedical Research Ethics Committee of Shanghai Institute of Nutrition and Health. The C57BL/6 miR-182 constitutive KO mice (52) were crossed with the C57BL/6 MMTV-PyMT mice, which were previously described (82). The miR-182 conditional KO (miR-182$^{fl/fl}$) mice were generated in C57BL/6 background by GemPharmtech and then crossed with *Lyz2-cre* mice (Shanghai Model Organisms Center).

For fat-pad injection assays, 5×10^4 Py8119, AT3 cells, or 4T1 were mixed with Matrigel (354234, BD Biosciences) and injected into the mammary fat pads on each side of 8-wk-old female mice. Syngenic immunocompetent C57BL/6 and BALB/C mice were used for Py8119/AT3 and 4T1, respectively. For macrophage depletion, 100 μL clodronate liposomes or PBS liposomes were injected into mammary fat pads of 8-wk-old female miR-182-KO or wild-type mice every 3 d. Py8119 cells were orthotopically transplanted as described previously at day 5. When tumors appeared, liposomes were injected into tumors every 3 d until the end of experiments. For analyses of Py8119 and BMDM coinjection, wild-type C57BL/6 female mice were irradiated by 4 Gy γ-rays, followed by injection of 100 μL clodronate liposome into the mammary glands 3 d later. Then, a mixture of 5×10^4 Py8119 cells and 2.5×10^5 miR-182-KO or wild-type BMDMs were injected into the mammary glands of the mice 4 d later. Bone marrow transplantation of mice was performed as described previously (83). Briefly, recipient C57BL/6 mice received lethal irradiation of 9 Gy γ-rays. Then, bone marrow cells from miR-182-KO or wild-type donors were resuspended in serum-free medium and injected into the tail vein of recipient mice 3 h later. After 1 mo, 5×10^4 Py8119 cells were orthotopically transplanted into the recipient mice.

Except for the MMTV-PyMT model, female mice aged 6 to 8 wk were used in all animal experiments. Unless stated otherwise, flow cytometry and IF analyses of transplanted tumors were performed 3 wk after orthotopic injection of the tumor cells. The flow cytometry and IF analyses of autochthonous tumors and serological analyses of the corresponding mice were performed 2 wk after the first palpable tumor. To analyze tumor invasiveness, hematoxylin and eosin staining was performed on tumor sections, and then Image J was used to measure the distance from the invasion front to the dense tumor edge (84).

Transcriptomic Sequencing and GSEA Analyses. The RNA of Py8119 transplanted tumors from miR-182-KO or wild-type mice, with three littermates for each group, were used for transcriptome sequencing. In addition, RNA was extracted from miR-182-KO or wild-type BMDMs and subjected to transcriptomic sequencing to analyze the molecular pathways affected by miR-182 in macrophages. For GSEA, all gene sets were obtained from Molecular Signatures Database (MSigDB, BROAD Institute).

Clinical Samples. Paraffin-embedded primary tumor specimens for the correlation analysis of miR-182 expression and CD206$^+$ cell infiltration levels were obtained from Qilu Hospital. Samples were obtained with informed patient consent and approval from the Research Review Board of the hospital.

Statistics and Reproducibility. The data presentation and statistical analyses are described in the figure legends. Data analyses were performed by GraphPad Prism 8 (GraphPad Software). The experiments in vitro were repeated independently at least three times with similar results. P values < 0.05 were considered as statistically significant.

Data Availability. The RNA sequencing data generated in this study have been deposited in the National Omics Data Encyclopedia (https://www.biosino.org/node, ID: OEP002515, OEP002516). The source data generated in this study are provided in Datasets S1–S4.

1. A. Ostman, The tumor microenvironment controls drug sensitivity. *Nat. Med.* **18**, 1332–1334 (2012).
2. D. F. Quail, J. A. Joyce, Microenvironmental regulation of tumor progression and metastasis. *Nat. Med.* **19**, 1423–1437 (2013).
3. B. Z. Qian, J. W. Pollard, Macrophage diversity enhances tumor progression and metastasis. *Cell* **141**, 39–51 (2010).
4. X. Zhuang, H. Zhang, G. Hu, Cancer and microenvironment plasticity: Double-edged swords in metastasis. *Trends Pharmacol. Sci.* **40**, 419–429 (2019).
5. S. K. Biswas, A. Mantovani, Macrophage plasticity and interaction with lymphocyte subsets: Cancer as a paradigm. *Nat. Immunol.* **11**, 889–896 (2010).
6. M. Stein, S. Keshav, N. Harris, S. Gordon, Interleukin 4 potently enhances murine macrophage mannose receptor activity: A marker of alternative immunologic macrophage activation. *J. Exp. Med.* **176**, 287–292 (1992).
7. S. Goerdt, C. E. Orfanos, Other functions, other genes: Alternative activation of antigen-presenting cells. *Immunity* **10**, 137–142 (1999).
8. C. D. Mills, K. Kincaid, J. M. Alt, M. J. Heilman, A. M. Hill, M-1/M-2 macrophages and the Th1/Th2 paradigm. *J. Immunol.* **164**, 6166–6173 (2000).
9. V. Goede, L. Brogelli, M. Ziche, H. G. Augustin, Induction of inflammatory angiogenesis by monocyte chemoattractant protein-1. *Int. J. Cancer* **82**, 765–770 (1999).
10. A. H. Lee, L. C. Happerfield, L. G. Bobrow, R. R. Millis, Angiogenesis and inflammation in invasive carcinoma of the breast. *J. Clin. Pathol.* **50**, 669–673 (1997).
11. L. Bingle, N. J. Brown, C. E. Lewis, The role of tumour-associated macrophages in tumour progression: Implications for new anticancer therapies. *J. Pathol.* **196**, 254–265 (2002).
12. F. J. Slack, A. M. Chinnaiyan, The role of non-coding RNAs in oncology. *Cell* **179**, 1033–1055 (2019).
13. J. Chen et al., miR-182 prevented ototoxic deafness induced by co-administration of kanamycin and furosemide in rats. *Neurosci. Lett.* **723**, 134861 (2020).
14. W. Ling, X. Xu, J. Liu, A causal relationship between the neurotherapeutic effects of miR182/7a and decreased expression of PRDM5. *Biochem. Biophys. Res. Commun.* **490**, 1–7 (2017).
15. Q. Wei, R. Lei, G. Hu, Roles of miR-182 in sensory organ development and cancer. *Thorac. Cancer* **6**, 2–9 (2015).

16. L. Zhang, T. Liu, Y. Huang, J. Liu, microRNA-182 inhibits the proliferation and invasion of human lung adenocarcinoma cells through its effect on human cortical actin-associated protein. *Int. J. Mol. Med.* **28**, 381–388 (2011).

17. X. Li *et al.*, Identification of new aberrantly expressed miRNAs in intestinal-type gastric cancer and its clinical significance. *Oncol. Rep.* **26**, 1431–1439 (2011).

18. I. K. Guttilla, B. A. White, Coordinate regulation of FOXO1 by miR-27a, miR-96, and miR-182 in breast cancer cells. *J. Biol. Chem.* **284**, 23204–23216 (2009).

19. L. Perilli *et al.*, Circulating miR-182 is a biomarker of colorectal adenocarcinoma progression. *Oncotarget* **5**, 6611–6619 (2014).

20. Z. Liu *et al.*, MiR-182 overexpression in tumourigenesis of high-grade serous ovarian carcinoma. *J. Pathol.* **228**, 204–215 (2012).

21. M. F. Segura *et al.*, Aberrant miR-182 expression promotes melanoma metastasis by repressing FOXO3 and microphthalmia-associated transcription factor. *Proc. Natl. Acad. Sci. U.S.A.* **106**, 1814–1819 (2009).

22. L. Jiang *et al.*, miR-182 as a prognostic marker for glioma progression and patient survival. *Am. J. Pathol.* **177**, 29–38 (2010).

23. B. D. McMillen *et al.*, Expression analysis of MIR182 and its associated target genes in advanced ovarian carcinoma. *Mod. Pathol.* **25**, 1644–1653 (2012).

24. K. Tsuchiyama *et al.*, Expression of microRNAs associated with Gleason grading system in prostate cancer: miR-182-5p is a useful marker for high grade prostate cancer. *Prostate* **73**, 827–834 (2013).

25. Z. Li *et al.*, miRNA-182 regulated MTSS1 inhibits proliferation and invasion in Glioma Cells. *J. Cancer* **11**, 5840–5851 (2020).

26. S. D. Weeraratne *et al.*, Pleiotropic effects of miR-183~96~182 converge to regulate cell survival, proliferation and migration in medulloblastoma. *Acta Neuropathol.* **123**, 539–552 (2012).

27. E. Yao, A. Ventura, A new role for miR-182 in DNA repair. *Mol. Cell* **41**, 135–137 (2011).

28. W. Lu, T. Lu, X. Wei, Downregulation of DNMT3a expression increases miR-182-induced apoptosis of ovarian cancer through caspase-3 and caspase-9-mediated apoptosis and DNA damage response. *Oncol. Rep.* **36**, 3597–3604 (2016).

29. Y. Q. Wang, R. D. Guo, R. M. Guo, W. Sheng, L. R. Yin, MicroRNA-182 promotes cell growth, invasion, and chemoresistance by targeting programmed cell death 4 (PDCD4) in human ovarian carcinoma. *J. Cell. Biochem.* **114**, 1464–1473 (2013).

30. C. H. Chiang, M. F. Hou, W. C. Hung, Up-regulation of miR-182 by beta-catenin in breast cancer increases tumorigenicity and invasiveness by targeting the matrix metalloproteinase inhibitor RECK. *Biochim. Biophys. Acta* **1830**, 3067–3076 (2013).

31. D. Wang, G. Lu, Y. Shao, D. Xu, MiR-182 promotes prostate cancer progression through activating Wnt/beta-catenin signal pathway. *Biomed. Pharmacother.* **99**, 334–339 (2018).

32. S. A. K. Rasheed, C. R. Teo, E. J. Beillard, P. M. Voorhoeve, P. J. Casey, MicroRNA-182 and microRNA-200a control G-protein subunit alpha-13 (GNA13) expression and cell invasion synergistically in prostate cancer. *J. Biol. Chem.* **288**, 7986–7995 (2013).

33. A. Spitschak, C. Meier, B. Kowtharapu, D. Engelmann, B. M. Putzer, MiR-182 promotes cancer invasion by linking RET oncogene activated NF-kappaB to loss of the HES1/Notch1 regulatory circuit. *Mol. Cancer* **16**, 24 (2017).

34. R. Lei *et al.*, Suppression of MIM by microRNA-182 activates RhoA and promotes breast cancer metastasis. *Oncogene* **33**, 1287–1296 (2014).

35. J. Yu *et al.*, MicroRNA-182 targets SMAD7 to potentiate TGFbeta-induced epithelial-mesenchymal transition and metastasis of cancer cells. *Nat. Commun.* **7**, 13884 (2016).

36. Y. Li *et al.*, MiR-182 inhibits the epithelial to mesenchymal transition and metastasis of lung cancer cells by targeting the Met gene. *Mol. Carcinog.* **57**, 125–136 (2018).

37. S. Zhang *et al.*, Circular RNA SFMBT2 inhibits the proliferation and metastasis of glioma cells through Mir-182-5p/Mtss1 pathway. *Technol. Cancer Res. Treat.* **19**, 1533033820945799 (2020).

38. M. Sachdeva *et al.*, MicroRNA-182 drives metastasis of primary sarcomas by targeting multiple genes. *J. Clin. Invest.* **126**, 1606 (2016).

39. H. Martinez-Ruiz *et al.*, A TGFbeta-miR-182-BRCA1 axis controls the mammary differentiation hierarchy. *Sci. Signal.* **9**, ra118 (2016).

40. F. M. Kouri *et al.*, miR-182 integrates apoptosis, growth, and differentiation programs in glioblastoma. *Genes Dev.* **29**, 732–745 (2015).

41. D. Yue, X. Qin, miR-182 regulates trastuzumab resistance by targeting MET in breast cancer cells. *Cancer Gene Ther.* **26**, 1–10 (2019).

42. Y. Sang *et al.*, circRNA_0025202 regulates tamoxifen sensitivity and tumor progression via regulating the miR-182-5p/FOXO3a axis in breast cancer. *Mol. Ther.* **27**, 1638–1652 (2019).

43. K.M. Kim *et al.*, miR-182 is a negative regulator of osteoblast proliferation, differentiation and skeletogenesis through targeting FoxO1. *J. Bone Miner. Res.* **27**, 1669–1679 (2012).

44. A. B. Stittrich *et al.*, The microRNA miR-182 is induced by IL-2 and promotes clonal expansion of activated helper T lymphocytes. *Nat. Immunol.* **11**, 1057–1062 (2010).

45. S. S. Myatt *et al.*, Definition of microRNAs that repress expression of the tumor suppressor gene FOXO1 in endometrial cancer. *Cancer Res.* **70**, 367–377 (2010).

46. L. Song *et al.*, TGF-beta induces miR-182 to sustain NF-kappaB activation in glioma subsets. *J. Clin. Invest.* **122**, 3563–3578 (2012).

47. Y. Qiu *et al.*, TGF-beta upregulates miR-182 expression to promote gallbladder cancer metastasis by targeting CADM1. *Mol. Biosyst.* **10**, 679–685 (2014).

48. P. Moskwa *et al.*, miR-182-mediated downregulation of BRCA1 impacts DNA repair and sensitivity to PARP inhibitors. *Mol. Cell* **41**, 210–220 (2011).

49. G. Li *et al.*, The microRNA-182-PDK4 axis regulates lung tumorigenesis by modulating pyruvate dehydrogenase and lipogenesis. *Oncogene* **36**, 989–998 (2017).

50. J. Xue *et al.*, Transcriptome-based network analysis reveals a spectrum model of human macrophage activation. *Immunity* **40**, 274–288 (2014).

51. W. Wang *et al.*, miR-100 maintains phenotype of tumor-associated macrophages by targeting mTOR to promote tumor metastasis via Stat5a/IL-1ra pathway in mouse breast cancer. *Oncogenesis* **7**, 97 (2018).

52. Z. B. Jin *et al.*, Targeted deletion of miR-182, an abundant retinal microRNA. *Mol. Vis.* **15**, 523–533 (2009).

53. O. M. Pello *et al.*, Role of c-MYC in alternative activation of human macrophages and tumor-associated macrophage biology. *Blood* **119**, 411–421 (2012).

54. G. Solinas *et al.*, Tumor-conditioned macrophages secrete migration-stimulating factor: A new marker for M2-polarization, influencing tumor cell motility. *J. Immunol.* **185**, 642–652 (2010).

55. S. Gordon, F. O. Martinez, Alternative activation of macrophages: Mechanism and functions. *Immunity* **32**, 593–604 (2010).

56. L. J. Bendall, K. F. Bradstock, G-CSF: From granulopoietic stimulant to bone marrow stem cell mobilizing agent. *Cytokine Growth Factor Rev.* **25**, 355–367 (2014).

57. X. Clemente-Casares *et al.*, Expanding antigen-specific regulatory networks to treat autoimmunity. *Nature* **530**, 434–440 (2016).

58. B. Jassal *et al.*, The reactome pathway knowledgebase. *Nucleic Acids Res.* **48**, D498–D503 (2020).

59. A. Jain *et al.*, Specific NEMO mutations impair CD40-mediated c-Rel activation and B cell terminal differentiation. *J. Clin. Invest.* **114**, 1593–1602 (2004).

60. V. Agarwal, G. W. Bell, J. W. Nam, D. P. Bartel, Predicting effective microRNA target sites in mammalian mRNAs. *eLife* **4**, e05005 (2015).

61. M. Kanehisa, M. Furumichi, Y. Sato, M. Ishiguro-Watanabe, M. Tanabe, KEGG: Integrating viruses and cellular organisms. *Nucleic Acids Res.* **49**, D545–D551 (2021).

62. S. L. Foster, D. C. Hargreaves, R. Medzhitov, Gene-specific control of inflammation by TLR-induced chromatin modifications. *Nature* **447**, 972–978 (2007).

63. J. Zhao *et al.*, Mesenchymal stromal cell-derived exosomes attenuate myocardial ischaemia-reperfusion injury through miR-182-regulated macrophage polarization. *Cardiovasc. Res.* **115**, 1205–1216 (2019).

64. R. Medzhitov *et al.*, MyD88 is an adaptor protein in the hToll/IL-1 receptor family signaling pathways. *Mol. Cell* **2**, 253–258 (1998).

65. K. A. Fitzgerald *et al.*, Mal (MyD88-adapter-like) is required for Toll-like receptor-4 signal transduction. *Nature* **413**, 78–83 (2001).

66. A. Kulkarni, *et al.* A designer self-assembled supramolecule amplifies macrophage immune responses against aggressive cancer. *Nat. Biomed. Eng.* **2**, 589 (2018).

67. Z. Belhadj *et al.*, A combined "eat me/don't eat me" strategy based on extracellular vesicles for anticancer nanomedicine. *J. Extracell. Vesicles* **9**, 1806444 (2020).

68. J. N. Pucella *et al.*, miR-182 is largely dispensable for adaptive immunity: Lack of correlation between expression and function. *J. Immunol.* **194**, 2635–2642 (2015).

69. Y. F. Li *et al.*, Loss of miR-182 affects B-cell extrafollicular antibody response. *Immunology* **148**, 140–149 (2016).

70. L. Wei *et al.*, Absence of miR-182 augments cardiac allograft survival. *Transplantation* **101**, 524–530 (2017).

71. O. R. Colegio *et al.*, Functional polarization of tumour-associated macrophages by tumour-derived lactic acid. *Nature* **513**, 559–563 (2014).

72. D. Namgaladze, B. Brune, Macrophage fatty acid oxidation and its roles in macrophage polarization and fatty acid-induced inflammation. *Biochim. Biophys. Acta* **1861**, 1796–1807 (2016).

73. Y. Bu *et al.*, Insulin regulates lipolysis and fat mass by upregulating growth/differentiation factor 3 in adipose tissue macrophages. *Diabetes* **67**, 1761–1772 (2018).

74. Y. Li *et al.*, Hypoxia-inducible miR-182 enhances HIF1alpha signaling via targeting PHD2 and FIH1 in prostate cancer. *Sci. Rep.* **5**, 12495 (2015).

75. B. Hu *et al.*, Therapeutic siRNA: State of the art. *Signal Transduct. Target. Ther.* **5**, 101 (2020).

76. E. V. Batrakova, M. S. Kim, Using exosomes, naturally-equipped nanocarriers, for drug delivery. *J. Control. Release* **219**, 396–405 (2015).

77. S. Kamerkar *et al.*, Exosomes facilitate therapeutic targeting of oncogenic KRAS in pancreatic cancer. *Nature* **546**, 498–503 (2017).

78. M. Cully, Exosome-based candidates move into the clinic. *Nat. Rev. Drug Discov.* **20**, 6–7 (2021).

79. G. Racchetti, J. Meldolesi, Extracellular vesicles of mesenchymal stem cells: Therapeutic properties discovered with extraordinary success. *Biomedicines* **9**, 667 (2021).

80. X. Zhuang *et al.*, Differential effects on lung and bone metastasis of breast cancer by Wnt signalling inhibitor DKK1. *Nat. Cell Biol.* **19**, 1274–1285 (2017).

81. W. Ying, P. S. Cheruku, F. W. Bazer, S. H. Safe, B. Zhou, Investigation of macrophage polarization using bone marrow derived macrophages. *J. Vis. Exp.*, 50323 (2013).

82. M. Cong *et al.*, MTSS1 suppresses mammary tumor-initiating cells by enhancing RBCK1-mediated p65 ubiquitination. *Nat. Can.* **1**, 222–234 (2020).

83. T. N. Small *et al.*, Comparison of immune reconstitution after unrelated and related T-cell-depleted bone marrow transplantation: Effect of patient age and donor leukocyte infusions. *Blood* **93**, 467–480 (1999).

84. Y. Liu *et al.*, Long non-coding RNA NR2F1-AS1 induces breast cancer lung metastatic dormancy by regulating NR2F1 and DeltaNp63. *Nat. Commun.* **12**, 5232 (2021).

12 of 12 | PNAS
https://doi.org/10.1073/pnas.2114006119

Ma et al.
miR-182 targeting reprograms tumor-associated macrophages and
limits breast cancer progression